Control of Acid−Base Properties of New Nanocomposite Derivatives of MCM-36 by Mixed Oxide Pillaring

Jan-Olaf Barth, Andreas Jentys, Jan Kornatowski, and Johannes A. Lercher*

Institute for Chemical Technology, Technische Universität München, Lichtenbergstrasse 4, 85747 Garching bei München, Germany

Received October 6, 2003. Revised Manuscript Received December 13, 2003

The layered precursor of zeolite MCM-22 was pillared with SiO_2, Al_2O_3, $MgO-Al_2O_3$, $BaO-Al_2O_3$, $Al_2O_3-SiO_2$, $MgO-Al_2O_3-SiO_2$, and $BaO-Al_2O_3-SiO_2$ to generate new derivatives of MCM-36. These nanocomposite materials are characterized by a layered structure consisting of microporous zeolite layers and mesoporous slit-shaped galleries formed by the incorporation of pure and mixed oxides between the zeolitic sheets. Enhanced Lewis acidity is generated by pillaring with (mixed) aluminum oxides. The adsorption of 2.6-di-*tert*-butylpyridine (2.6-DTBPy) demonstrated for all materials an increased accessibility to acid sites at the pore mouth or the outer surface of the zeolite layers compared to MCM-22. For $(MgO/BaO)-Al_2O_3-SiO_2$−MCM-36 additional Brønsted acid sites of higher strength than the sites in the zeolitic sheets are observed, which are assigned to the silica−alumina clusters in the interlayer galleries. Basic properties were introduced by the incorporation of alkaline earth oxide aluminates ($MgO/BaO-Al_2O_3$) into the interlayer space. Two basic hydroxyl functions were detected by CO_2 adsorption: (i) Mg(Ba)-OH and (ii) Al_{IV}-OH groups on the spinel-type oxide clusters. The latter basic sites are attributed to hydroxyl groups on aluminum ions in a tetrahedral coordination sphere of the defect spinel-type oxide pillaring clusters.

Introduction

Zeolites are solid acid catalysts which are used commercially in over 70 industrial processes.[1,2] Because of their well-defined pores with minimum kinetic diameters of the size of small organic molecules, zeolites can be used as shape-selective catalysts.[2] Nevertheless, especially for petrochemical applications, solid acids are required to catalyze reactions involving larger, bulkier molecules. In this respect two classes of materials are of special interest: (i) mesoporous M41S-type materials and (ii) pillared or delaminated layered materials, such as clays and zeolites. The M41S family has been extensively investigated regarding the formation and characterization of the porous structure.[3,4] Many catalytic applications have been reported for MCM-41-related materials or modifications thereof.[4] However, the acid sites in these materials show significantly weaker acid strength than the Brønsted acid sites (bridging hydroxyl groups) in zeolites.[5,6] Thus, materials with acid sites of strength similar to those in zeolites, which are accessible to large organic molecules, are of general interest. In this respect, pillared or delaminated layered materials offer promising possibilities.[7] Potential applications of the materials are, in principle, all types of reactions that require catalysts with more than one functionality, e.g. the combination of acid/base properties with redox or metallic sites.[2,3,8]

In this paper, the acid−base properties of novel MCM-36 derivatives with aluminum-based binary oxides pillars such as Al_2O_3, $MgO-Al_2O_3$, $BaO-Al_2O_3$, $Al_2O_3-SiO_2$, $MgO-Al_2O_3-SiO_2$, and $BaO-Al_2O_3-SiO_2$ are discussed. A thorough physicochemical characterization is presented, providing deeper insights into the complex transformations leading to new nanocomposite derivatives of MCM-36. Features resulting from the combination of mesoporosity with zeolitic microporosity and the acid−base character are discussed.

Experimental Section

Synthesis of MCM-36 Derivatives. MCM-22 and SiO_2−MCM-36 were synthesized according to the procedure described by He et al.,[8] which is based on the synthesis described by Roth et al.[9] An uncalcined precursor (wet cake) of MCM-22 (Si/Al = 12), which was synthesized under rotating conditions, was used for all syntheses.

Synthesis of Al_2O_3−MCM-36, $MgO-Al_2O_3$−MCM-36, and $BaO-Al_2O_3$−MCM-36. The swelling process was identical for all samples, following the procedure described by He and Barth et al.[8,10,11] A wet cake of the uncalcined precursor of MCM-22 (containing 25−30% solids) was mixed with hexadecyltri-

* To whom correspondence should be addressed. Fax: (+49) 89 28913544. E-mail: johannes.lercher@ch.tum.de.

(1) Weitkamp, J. *Solid State Ionics* **2000**, *131*, 175.
(2) Lercher, J. A.; Jentys, A. In *Handbook of Microporous Solids*; Schüth, F., Sing, K., Weitkamp, J., Eds.; Wiley-VCH: Weinheim, Germany, 2002; p 1097.
(3) Ciesla, U.; Schüth, F. *Microporous Mesoporous Mater.* **1999**, *27*, 131.
(4) Ying, J. Y.; Mehnert, C. P.; Wong, M. S. *Angew. Chem. Int. Ed.* **1999**, *38*, 56.
(5) Jentys, A.; Pham, N. H.; Vinek, H. *J. Chem. Soc., Faraday Trans.* **1996**, *92*, 3287.
(6) Jentys, A.; Kleestorfer, K.; Vinek, H. *Microporous Mesoporous Mater.* **1999**, *27*, 321.
(7) Gil, A.; Gandía, L. M. *Catal. Rev.-Sci. Eng.* **2000**, *42*, 145.
(8) He, Y. J.; Nivarthy, G. S.; Eder, F.; Seshan, K.; Lercher, J. A. *Microporous Mesoporous Mater.* **1998**, *25*, 207.
(9) Roth, W. J.; Kresge, C. T.; Vartuli, J. C.; Leonowicz, M. E.; Fung, A. S.; McCullen, S. B. *Stud. Surf. Sci. Catal.* **1995**, *94*, 301.

10.1021/cm0349607 CCC: $27.50
Published on Web 01/21/2004

Table 1. Elemental Composition and BET Surface Areas of Derivatives of MCM-36 and the MCM-22 Parent Material

sample	Si [wt %]	Al [wt %]	Na [wt %]	Mg [wt %]	Ba [wt %]	BET surface area [m^2/g]
MCM-22	45.40	3.85	0.25			432
Al_2O_3−MCM-36	36.49	5.65	<0.10			357
MgO−Al_2O_3−MCM-36	27.92	21.28	<0.10	0.64		348
BaO−Al_2O_3−MCM-36	9.33	35.90	<0.10		2.20	390
SiO_2−MCM-36	43.05	1.61	<0.10			711
Al_2O_3−SiO_2−MCM-36	41.67	3.91	<0.10			584
MgO−Al_2O_3−SiO_2−MCM-36	39.90	4.32	<0.10	0.24		757
BaO−Al_2O_3−SiO_2−MCM-36	40.06	4.48	<0.10		0.24	689

methylammonium chloride (CTMACl, 25% solution) and tetrapropylammonium hydroxide (TPAOH, 20% solution) at weight ratios of 1:4:1.2. The mixture was adjusted to pH = 13.5 and reacted under continuous stirring at 373 K for 68 h followed by agitation at room temperature for 4 h. The resulting swollen material was filtered, washed with a small amount of water, and dried at ambient conditions. The solutions for pillaring with alumina were prepared as follows: a NaOH solution (720 mL, 0.2 M, Fluka) was added dropwise to an $AlCl_3$ solution (720 mL, 0.1 M, Merck) under stirring. The mixture was agitated at 363 K for 4 h and finally aged at 298 K for 60 h. For pillaring with MgO−Al_2O_3 and BaO−Al_2O_3, to the same Al solution as described above (after aging for 60 h), MgO (1.45 g, Aldrich), respectively BaO (5.52 g, Fluka), was slowly added under stirring [molar ratio Mg-(Ba)/Al/OH = 1:2:4] and the resulting mixture was agitated at room temperature overnight. Pillaring was performed by addition of the swollen MCM-22 precursor (3 g in a 10 wt % water suspension) to the pillaring solution (ca. 24 mmol Al/g swollen MCM-22 precursor). The mixture was heated at 353 K under stirring for 25 h. The products were filtered, dried at room temperature overnight, and calcined at 723 K (ramp 1 K min^{-1}) under N_2 flow (100 mL min^{-1}) for 6 h, and subsequently at 823 K (ramp 2 K min^{-1}) in synthetic air (100 mL min^{-1}) for 12 h.

Synthesis of Al_2O_3−SiO_2−MCM-36, MgO−Al_2O_3−SiO_2−MCM-36, and BaO−Al_2O_3−SiO_2−MCM-36. In analogy to the synthesis of SiO_2−MCM-36, the swollen MCM-22 was mixed with TEOS (tetraethoxysilane, Merck) at a weight ratio of 1:5, heated at 351 K under N_2 and stirred for 25 h, then filtered and dried at room temperature. The resulting solid was hydrolyzed with solutions of $AlCl_3$−NaOH and MgO/BaO−$AlCl_3$−NaOH (preparation of pillaring solutions cf. above) at 313 K as suspension in water (wt. ratio 1:10) of pH 8 (controlled with NaOH) for 6 h, then filtered, dried at 300 K, and calcined at 723 K under N_2 flow (100 mL min^{-1}) for 6 h, and finally at 823 K under air for 12 h.

Characterization. The elemental compositions of the samples were obtained using atomic absorption spectroscopy (AAS) with a UNICAM 939 AA-spectrometer. Energy-dispersive X-ray fluorescence (EDX) measurements were carried out using a JEOL 500 scanning electron microscope equipped with a Röntec EDX-spectrometer. Nitrogen adsorption measurements were performed at 77.4 K with a PMI automated BET sorptometer 5.32. The samples were outgassed at 673 K and 10^{-3} Pa for 24 h prior to the adsorption measurements. The specific surface areas were calculated by the Brunauer−Emmet−Teller (BET) method. The micropore volume was calculated from t-plots using the Harkins−Jura equation. ^{27}Al magic angle spinning (MAS) NMR was measured on a BRUKER MSL-300 spectrometer (7.05 T) at 78.205 MHz. The spectra were obtained from samples pressed into 4-mm zirconia rotors at a spin rate of 13 kHz using a $\pi/12$ pulse of 1 μs and a recycle delay of 2 s. IR spectra were recorded in situ during activation, adsorption, and temperature- programmed desorption at a resolution of 4 cm^{-1} (Bruker IFS-88). The samples were pressed into thin, self-supporting wafers and activated in a vacuum ($p < 10^{-6}$ mbar) at 723 K (10 $Kmin^{-1}$ ramp) for 60 min. Pyridine and 2.6-di-*tert*-butyl-pyridine (2.6-DTBPy) were adsorbed at 373 K with partial pressures of 10^{-3} to 10^{-2} mbar and desorbed by heating the sample from 373 to 723 K in a vacuum ($p < 10^{-6}$ mbar). CO_2 was adsorbed at 308 K with partial pressures of 10^{-3} to 1 mbar and desorbed by heating from 308 to 723 K in a vacuum ($p < 10^{-6}$ mbar). All spectra were normalized to the integral peak area of the overtones of the framework vibrations in the range of 2110−1735 cm^{-1}. Temperature-programmed desorption (TPD) of ammonia was used for determining the concentrations of acid sites in the samples. The sample (~100 mg) was degassed by evacuating to 10^{-3} mbar, followed by heating at a rate of 10 K min^{-1} to 723 K, and maintaining at that temperature for 60 min. After the sample was cooled to 373 K, it was equilibrated with 1 mbar of ammonia for 60 min. Subsequently the system was evacuated to 10^{-3} mbar for 180 min and heated to 850 K at a rate of 10 $Kmin^{-1}$. During this temperature ramp, mass spectra of the gas phase were collected at 5-K intervals using a QMG 420 mass spectrometer to determine the rate of ammonia desorption.

Results and Discussion

Materials. Table 1 summarizes the elemental composition and the BET surface areas of the derivatives of MCM-36 investigated in this study. The XRD patterns (not shown) of the samples correspond well to those reported in the literature for MCM-36.[8,9,12−15] A detailed physicochemical characterization of the textural properties of such nanocomposite materials can be found in ref 11.

The Si/Al ratio strongly increases as the result of the transformation from MCM-22 to SiO_2−MCM-36, which is indicative of an intercalation of SiO_2 moieties between the MCM-22 layers and/or a partial dealumination of the zeolite framework during the pillaring process. In contrast, the Si/Al ratio decreases significantly to Si/Al < 10 upon pillaring with the alumina species, which indicates a high amount of alumina to be retained in the composite materials. Note, that for MgO−Al_2O_3−SiO_2−MCM-36 and BaO−Al_2O_3−SiO_2−MCM-36 higher concentrations of Al have been retained in the composite materials as compared to those in Al_2O_3−SiO_2−MCM-36. This results from the addition of basic alkali earth oxides to the pillaring solutions, which leads to an increase of the pH value from 4.5 to 5.5 and results in a higher concentration of polyoxocationic Al species, such as the Keggin cation $[Al_{13}O_4(OH)_{24}(H_2O)_{12}]^{7+}$ due to base-induced condensation processes of the polyoxocationic, octahedrally coordinated Al species.

(10) Barth, J.-O.; Schenkel, R.; Kornatowski, J.; Lercher, J. A. *Stud. Surf. Sci. Catal.* **2001**, *135*, 136.
(11) Barth, J.-O.; Kornatowski, J.; Lercher, J. A. *J. Mater. Chem.* **2002**, *12*, 369.
(12) Fung, A. S.; Lawton, S. L.; Roth, W. J. U.S. Patent 5362697, 1994.
(13) Eder, F.; He, Y. J.; Nivarthy, G. S.; Lercher, J. A. *Recl. Trav. Chim. Pays−Bas Belg.* **1996**, *115*, 531.
(14) Corma, A.; Fornes, V.; Martinez-Triguero, J.; Pergher, S. B. *J. Catal.* **1999**, *186*, 57.
(15) Roth, W. J.; Vartuli, J. C.; Kresge, C. T. *Stud. Surf. Sci. Catal.* **2000**, *129*, 501.

Table 2. ^{27}Al-MAS NMR Data for Nanocomposite Materials Based on MCM-22

sample	δ Al (Al_{Td})	δ Al (Al_{Ph})	δ Al (Al_{Oh})	% Al (Al_{Td})	% Al (Al_{Ph})	% Al (Al_{Oh})
MCM-22	55.2		−0.5	87.2		12.8
Al_2O_3−MCM-36	51.8	33.5	−1.0	47.3	7.8	44.9
MgO−Al_2O_3−MCM-36	63.7		4.6	19.3		80.7
BaO−Al_2O_3−MCM-36	62.2		4.6	24.4		75.6
SiO_2−MCM-36	51.6	29.6	−1.0	66.9	3.6	29.5
Al_2O_3−SiO_2−MCM-36	52.1	26.3	−0.8	65.3	4.3	30.4
MgO−Al_2O_3−SiO_2−MCM-36	52.7		−1.0	62.3		37.7
BaO−Al_2O_3−SiO_2−MCM-36	52.4	27.9	−1.3	57.5	8.8	33.7

^{27}Al-MAS NMR. ^{27}Al-MAS NMR spectroscopy was used to determine the nature and the coordination of Al species in the investigated materials. Figure 1 shows

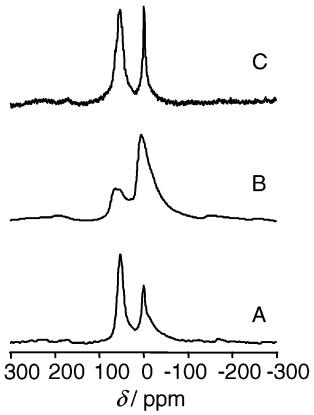

Figure 1. ^{27}Al-MAS NMR spectra of (A) Al_2O_3−MCM-36, (B) BaO−Al_2O_3−MCM-36, and (C) MgO−Al_2O_3−SiO_2−MCM-36.

three examples of ^{27}Al-MAS NMR spectra typical of MCM-36 derivatives (Al_2O_3−MCM-36, BaO−Al_2O_3−MCM-36, and MgO−Al_2O_3−SiO_2−MCM-36). Two main signals characteristic of aluminum species in a tetrahedral (Al_{Td}, ∼50 ppm) and an octahedral coordination sphere (Al_{Oh}, ∼0 ppm) can be distinguished.[16] Unverricht et al.[17] and Lawton et al.[18] have shown by the use of high-field (17.6 T) NMR that the resonance at ∼50 ppm is comprised of three T_d signals (∼50, ∼56, and ∼61 ppm), corresponding to distinct T_d Al species in the framework of MCM-22. The NMR spectra of all investigated nanocomposite materials have been deconvoluted using a superposition of multiple Lorentzian peaks. In addition to Al_{Td} and Al_{Oh} species, some of the materials show a third resonance at ∼30 ppm, which is tentatively attributed to pentahedrally coordinated aluminum. Such species may occur at the outer termination of the aluminum oxide clusters, or they may be due to not fully hydrated aluminum species in the oxide pillars. The relative percentage of the various types of aluminum is given in Table 2.

Note that upon intercalation of (mixed) aluminum oxide pillars between the zeolite layers the amount of aluminum in octahedral (pentahedral) coordination increased significantly. The pillaring solutions used in the transformation reactions contain polyoxocationic Al ions (e.g., Al_{13} Keggin units), consisting of aggregated aluminum-hydroxide octaeders. Calcination leads to a dehydroxylation of such clusters creating aluminum oxides with octahedrally coordinated aluminum (defective spinel structure). For MgO/(BaO)−Al_2O_3−MCM-36 the fraction of Al_{Oh} species is significantly higher compared to that of the other nanocomposite materials. The presence of alkaline earth oxides seems to enhance the formation of spinel-type clusters between the MCM-22 layers. The existence of such pillars is demonstrated by a characteristic low field shift of the maximum of the Al_{Td} (63.7 ppm) and Al_{Oh} (4.6 ppm) resonances.[19] Deconvolution of the spectra yields, in addition to the Al_{Td} resonance of framework aluminum in the zeolite phases (∼50 ppm), a second resonance at ∼68 ppm. This peak is tentatively assigned to tetrahedrally coordinated aluminum species in the (defect) spinel structure of the MgO/(BaO)−Al_2O_3 clusters.[19] Consequently, the significant increase of the amount of octahedrally coordinated aluminum is attributed to Al ions occupying octahedral interstitial sites in the alumina phases. The broad and slightly asymmetric line shape of the peak hints at a distribution of various aluminum species in an octahedral coordination sphere. However, part of these types of aluminum may be due to a dealumination of the zeolite layers during the swelling, pillaring, and calcination process.

IR Spectroscopy and Measurement of Acidity. Infrared spectra of the investigated materials in activated form show typical bands of OH stretching vibrations of surface hydroxyl groups (Figure 2) in the range

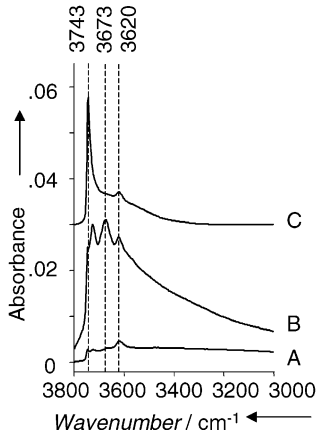

Figure 2. IR spectra of the hydroxyl region of (A) MCM-22, (B) MgO−Al_2O_3−MCM-36, and (C) MgO−Al_2O_3−SiO_2−MCM-36 (T = 373 K, 10^{-7} mbar) measured after in situ activation.

of 3650−3750 cm^{-1}. The bands at 3743 and 3725 cm^{-1}

(16) Kennedy, G. J.; Lawton, S. L.; Fung, A. S.; Rubin, M. K.; Steuernagel, S. *Catal. Today* **1999**, *49*, 385.
(17) Unverricht, S.; Hunger, M.; Ernst, S.; Karge, H. G.; Weitkamp, J. *Stud. Surf. Sci. Catal.* **1994**, *84*, 37.
(18) Lawton, S. L.; Fung, A. S.; Kennedy, G. J.; Alemany, L. B.; Chang, C. D.; Hatzikos, G. H.; Lissy, D. N.; Rubin, M. K.; Timken, H.-K. C.; Steuernagel, S.; Woessner, D. E. *J. Phys. Chem.* **1996**, *100*, 3788.
(19) Lee, M.-H.; Cheng, C.-F.; Heine, V.; Klinowski, J. *Chem. Phys. Lett.* **1997**, *265*, 673.

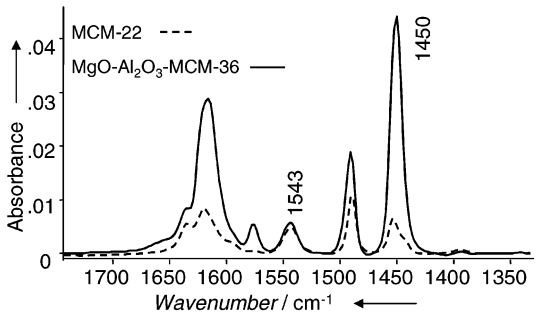

Figure 3. Difference IR spectra of MCM-22 and $MgO-Al_2O_3-$MCM-36 after adsorption of pyridine [p_{ads} (Pyr.) = 10^{-2} mbar, T_{ads} = 373 K, degassing at 373 K, 10^{-7} mbar, 60 min].

are assigned to terminal and internal Si−OH groups of the MCM-22 layers, respectively, whereas those at 3665 cm^{-1} are attributed to OH-groups of extraframework aluminum species.[8,13] The band at 3620 cm^{-1} is assigned to strong Brønsted acidic bridging hydroxyl groups. Note that for samples pillared with TEOS a significant increase of intensity of the silanol band at 3743 cm^{-1} was observed, which is indicative of Si−OH groups located on the outer termination of SiO_2 pillars present between the zeolite layers. Using MgO (BaO) as additional pillaring agents creates an intense band at ~3726 (3724) cm^{-1} which is attributed to Mg−OH (Ba−OH) groups in the spinel-type mixed oxide pillars.[20] For all nanocomposite materials in which (mixed) aluminum oxides have been incorporated between the zeolite layers, a higher concentration of Al−OH groups is observed compared to that in MCM-22 and SiO_2-MCM-36 as indicated by intense bands with maxima in the range of 3670−3680 cm^{-1}.

IR spectroscopy of pyridine adsorption was used to probe the type and concentrations of acid sites present on the MCM-36 type materials. The IR bands are assigned to the ring-bending vibrations of pyridinium ions and pyridine coordinatively bound to Lewis acid sites.[10,21,22] Difference IR spectra, recorded after reaching adsorption/desorption equilibrium at 10^{-2} mbar pyridine pressure and evacuating at 373 K for 60 min to remove physisorbed pyridine, are shown in Figure 3. For MCM-22 bands at 1540 and 1453 cm^{-1} (shoulder at 1443 cm^{-1}) indicating protonated pyridine on Brønsted acid sites and pyridine coordinatively bound to Lewis acid sites are observed. The latter band can be assigned to the interaction of pyridine with sodium cations present in the as-synthesized material (shoulder at 1443 cm^{-1}) and with extraframework aluminum (1453 cm^{-1}), respectively. For $MgO-Al_2O_3-$MCM-36 and MCM-22 nearly identical concentrations of Brønsted acid sites accessible for pyridine have been determined, whereas the concentration of Lewis acid sites due to (extraframework) aluminum oxides has significantly increased. The ratio between Brønsted and Lewis acid sites (cf. Table 3) has been calculated using extinction coefficients determined by Emeis.[23] Note that the concentration of Lewis acid sites has considerably increased in all materials containing aluminum oxides in the interlayer space. It has to be pointed out that

Table 3. Ratio of Brønsted and Lewis Acid Site Concentrations Determined from Pyridine Adsorption [p_{ads} (Pyr.) = 10^{-2} mbar, T_{ads} = 373 K, Degassing at 373 K, 10^{-7} mbar, 60 min.]

sample	C_{BA}/C_{LA}
MCM-22	1.16
Al_2O_3-MCM-36	0.81
$MgO-Al_2O_3-$MCM-36	0.18
$BaO-Al_2O_3-$MCM-36	0.11
SiO_2-MCM-36	1.27
$Al_2O_3-SiO_2-$MCM-36	0.58
$MgO-Al_2O_3-SiO_2-$MCM-36	1.04
$BaO-Al_2O_3-SiO_2-$MCM-36	0.83

aluminum acting as Lewis acid sites may not only be due to the intercalation of (mixed) aluminum oxides acting as pillars, but also to a dealumination of the zeolite layers as a result of the calcination and the swelling and/or pillaring procedure.

IR investigations of the adsorption of 2.6-di-*tert*-butylpyridine (2.6-DTBPy) were used to probe the acidic properties and to distinguish between acid sites inside the pores and sites on the externally accessible surface of the layered materials.[24] Because of its larger kinetic diameter, 2.6-DTBPy can adsorb only at the pore openings or at the external surface of the zeolitic materials, but cannot penetrate into the pore system of MCM-22.[25,26] Pyridine, however, easily diffuses into the 10- and 12-membered ring (MR) channels and interacts with the acid sites in channels and cavities.[27,28]

Adsorbed 2.6-DTBPy exhibits several bands in the regions of 3400−2800 cm^{-1} and 1710−1350 cm^{-1}, assigned to stretching and bending vibrations, respectively, analogous to pyridine.[29] The bands at 3365, 1616, and 1530 cm^{-1} are characteristic signals for the DTBPyH$^+$ ion. For the comparison of the external surface acidity, the band at ~3365 cm^{-1} assigned to the $\nu(N-H^+)$ stretching vibration of the DTBPyH$^+$ ion (which can be related to the presence of Brønsted acid sites on the external surface or the pore mouth[25]) has been followed (Figure 4). Table 4 compiles an overview of the intensities of the band of the $\nu(N-H^+)$ stretching vibration in the investigated materials in relation to that of MCM-22.

Exfoliation of the zeolite layers and intercalation of (mixed) oxides has increased significantly the accessibility of acid sites on the pore mouth (external surface) of the zeolite phases to the sterically demanding probe molecule 2.6-di-*tert*-butyl-pyridine. Note that for $Al_2O_3-SiO_2-$MCM-36 and MgO (BaO)$-Al_2O_3-SiO_2-$MCM-36 the concentration of Brønsted acid sites accessible for 2.6-DTBPy is considerably larger than for the other MCM-36 type materials. This observation might be explained with additional Brønsted acid sites on the oxide pillars between the zeolite sheets. In contrast to SiO_2-MCM-36, for Al_2O_3-MCM-36 and MgO(BaO)$-Al_2O_3-$MCM-36 the hydrolysis of TEOS has been per-

(20) Lercher, J. A. *Z. Phys. Chem.* **1982**, *129*, 209.
(21) Hughes, T. R.; White, H. M. *J. Phys. Chem.* **1967**, *71*, 2192.
(22) Ward, J. W.; Hansford, R. C. *J. Catal.* **1969**, *13*, 364.
(23) Emeis, C. A. *J. Catal.* **1993**, *141*, 347.
(24) Zheng, S.; Heydenrych, H. R.; Jentys, A.; Lercher, J. A. *J. Phys. Chem. B.* **2002**, *106*, 9552.
(25) Corma, A.; Fornés, V.; Forni, L.; Márquez, F.; Martínez-Triguero, J.; Moscotti, D. *J. Catal.* **1998**, *179*, 451.
(26) Schenkel, R.; Barth, J.-O.; Kornatowski, J.; Lercher, J. A. *Stud. Surf. Sci. Catal.* **2002**, *142*, 69.
(27) Corma, A.; Corell, C.; Perez-Pariente, J. *Zeolites* **1995**, *15*, 2.
(28) Meloni, D.; Laforge, S.; Martin, D.; Guisnet, M.; Rombi, E.; Solinas, V. *Appl. Catal. A* **2001**, *215*, 55.
(29) Knözinger, H.; Krietenbrink, H.; Ratnasamy, P. *J. Catal.* **1977**, *48*, 436.

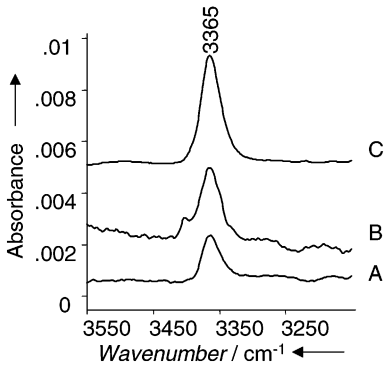

Figure 4. Difference IR spectra of (A) MCM-22, (B) MgO−Al_2O_3−MCM-36, and (C) MgO−Al_2O_3−SiO_2−MCM-36 after adsorption of 2.6-di-*tert*-butyl-pyridine [p_{ads} (2.6-DTBPY) = 10^{-2} mbar, T_{ads} = 373 K, degassing at 373 K, 10^{-7} mbar, 60 min].

Table 4. Adsorption of 2.6-di-*tert*-Butyl-pyridine (2.6-DTPy) at 10^{-2} mbar and 373 K; Relative Areas of the Band at 3365 cm^{-1} Assigned to the $\nu(N - H^+)$ Stretching Vibration of the $DTBPyH^+$ Ion

sample	A_{3365} (a.u.)
MCM-22	1.00
Al_2O_3−MCM-36	1.39
MgO−Al_2O_3−MCM-36	1.73
BaO−Al_2O_3−MCM-36	1.46
SiO_2−MCM-36	1.51
Al_2O_3−SiO_2−MCM-36	2.50
MgO−Al_2O_3−SiO_2−MCM-36	2.40
BaO−Al_2O_3−SiO_2−MCM-36	2.33

Table 5. Acid Site Concentrations Determined from Temperature-Programmed Desorption (TPD) of NH_3

sample	acid site concentration (mmol/g)
MCM-22	0.79
Al_2O_3−MCM-36	1.10
MgO−Al_2O_3−MCM-36	0.91
BaO−Al_2O_3−MCM-36	0.31
SiO_2−MCM-36	0.19
Al_2O_3−SiO_2−MCM-36	0.25
MgO−Al_2O_3−SiO_2−MCM-36	0.42
BaO−Al_2O_3−SiO_2−MCM-36	0.38

formed with water solutions containing polyoxocationic aluminum cations. Thus, the hydrolysis and subsequent calcination will create additional Si−OH−Al Brønsted sites on the (mixed) oxide pillars. Such acid sites should be easily accessible for 2.6-DTBPy as the probe molecule can diffuse into the mesoporous interlayer galleries without major sterical hindrance.

Temperature-Programmed Desorption (TPD) of Ammonia. The concentration and distribution of acid sites in MCM-22 and MCM-36 derivatives after activation at 723 K were characterized by temperature-programmed desorption (TPD) of ammonia (cf. Table 5, Figure 5). The TPD profiles of ammonia from parent MCM-22 and MCM-36 derivatives showed a maximum at 608 K, a shoulder at ∼498 K, and a characteristic shoulder in the range of 720−850 K. Unverricht et al.[17] and He et al.[8] attributed the first shoulder to physisorbed ammonia desorbing from the samples, whereas the partially overlapped maximum at approximately 608 K is assigned to the desorption of NH_4^+ ions from strong Brønsted acid sites. The broad shoulder (720−850 K) is ascribed to strong Lewis acid sites (extraframework aluminum species) generated during the swelling and calcination procedure.

The acid site concentration of SiO_2−MCM-36 is significantly lower compared to MCM-22 (not pillared reference material). This observation can be explained by the lower concentration of aluminum due to the incorporation of SiO_2 pillars into this sample. However, in Al_2O_3−MCM-36 and MgO−Al_2O_3−MCM-36, the intercalation of (mixed) aluminum oxides between the zeolite layers led to an increase of the total acid site concentration. In comparison to the MCM-22 parent material the more pronounced shoulder in the range of 720−850 K indicates that the higher acidity of these samples can be explained by the generation of strong Lewis acid sites on the aluminum oxide phases between the zeolite sheets. Note that BaO−Al_2O_3−MCM-36 (acid site concentration: 0.31 mmol/g) shows a far more basic character than MgO−Al_2O_3−MCM-36 (0.91 mmol/g). The lower intensity of the maximum at 608 K, and the shoulder above 670 K hints at a significantly lower concentration of Brønsted and Lewis acid sites in this material. This observation might be explained with a partial Ba ion exchange of the Brønsted acid sites and a distinct nature of the less Lewis acidic BaO−Al_2O_3 oxide clusters compared to MgO−Al_2O_3 pillars. For the MCM-36 derivatives with SiO_2 moieties between the zeolite layers, a systematic increase of acidity can be observed after incorporation of (mixed) aluminum oxides into the SiO_2 phases. Interestingly, not only the concentration of Lewis acid sites due to extraframework aluminum oxides increased, but also the maximum characteristic of Brønsted acid sites shifted to higher temperatures. This observation is tentatively explained by the generation of new stronger Si−OH−Al Brønsted acid sites by the hydrolysis of tetraethoxysilane (TEOS) with the aluminum-containing pillaring solutions. Consequently, such Brønsted acid sites should also exist on the oxide pillars between the zeolite layers.

CO_2 Adsorption. Using binary mixed alkaline earth-aluminum oxides as pillaring agents, the transformation of MCM-22 zeolite precursor into derivatives of MCM-36 creates nanocomposite materials with acid *and* basic properties. As discussed above Brønsted acid sites are generally found in the zeolite layers, whereas strong Lewis acid sites are formed by Al_2O_3 clusters in the interlayer galleries (accompanied by certain amounts of extraframework aluminum). Basic sites can be generated by the introduction of alkaline earth oxide clusters (e.g., MgO, BaO) as pillars between the MCM-22 sheets. To investigate the basic character of the nanocomposite materials, CO_2 adsorption has been followed by IR spectroscopy. Figure 6 shows IR spectra obtained after adsorption of CO_2 at 308 K on MgO−Al_2O_3−SiO_2−MCM-36 and MgO(BaO)−Al_2O_3−MCM-36. In the range of 1380−1700 cm^{-1} various bands characteristic of carbonate species appear upon admission of CO_2. Bands characteristic of uni- (1410, 1540−1580 cm^{-1}) and bidentate carbonates (1380, 1700 cm^{-1}) as well as bicarbonate species (1446, 1646 cm^{-1}) have been identified.[30,31] Note that due to the lower amount of MgO in MgO−Al_2O_3−SiO_2−MCM-36 and the higher average electronegativity, the concentration of basic sites is significantly lower than for MgO−Al_2O_3−MCM-36. The

(30) Philipp, R.; Fujimoto, K. *J. Phys. Chem.* **1992**, *96*, 9035.
(31) Lercher, J. A.; Colombier, C.; Noller, H. *J. Chem. Soc., Faraday Trans. 1* **1984**, *80*, 949.

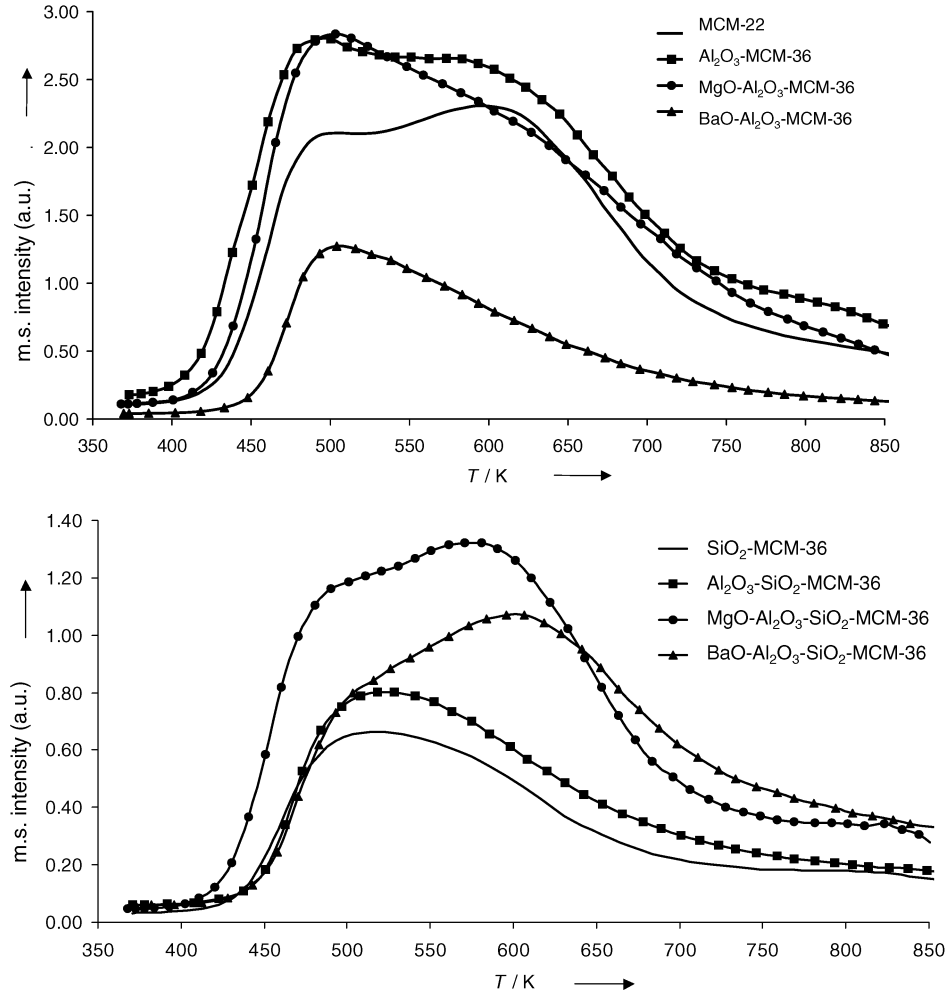

Figure 5. Temperature-programmed desorption of NH_3 from MCM-22 and derivatives of MCM-36 [ramp 10 K/min, activation at 723 K, p_{ads} (NH_3) = 1 mbar, T_{ads} = 373 K, degassing at 373 K, 10^{-7} mbar, 180 min].

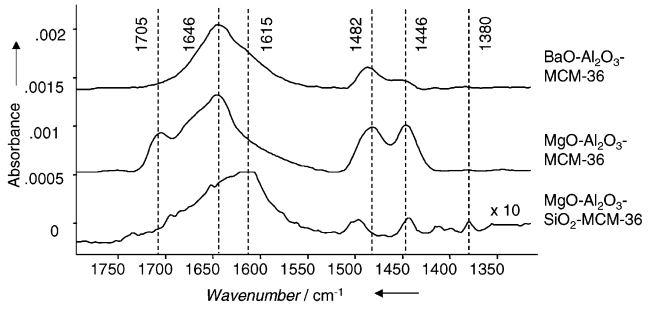

Figure 6. Difference IR spectra of MCM-36 derivatives after adsorption of CO_2 [p_{ads} (CO_2) = 1 mbar, T_{ads} = 308 K, degassing at 308 K, 10^{-7} mbar, 60 min].

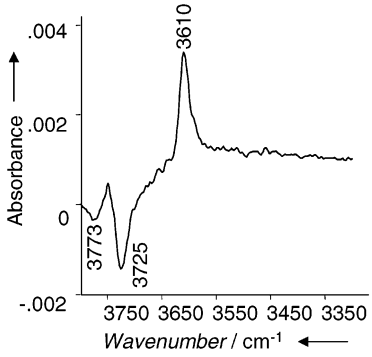

Figure 7. Difference IR spectrum of $MgO-Al_2O_3-MCM-36$ after adsorption of CO_2 [p_{ads} (CO_2) = 1 mbar, T_{ads} = 308 K, degassing at 308 K, 10^{-7} mbar, 60 min].

presence of bicarbonate species is concluded from the appearance of a band at 3610 cm^{-1}, which is assigned to the bicarbonate hydroxyl group.[31]

Figure 7 demonstrates that upon adsorption of CO_2 on $MgO(BaO)-Al_2O_3-MCM-36$ (spectrum for $BaO-Al_2O_3-MCM-36$ not shown) the formation of the band at 3610 cm^{-1} is accompanied by a loss of intensity of hydroxyl bands at 3725 and 3773 cm^{-1}. This observation points to a reaction of CO_2 with basic Mg−OH groups (3725 cm^{-1}) in the interlayer phase yielding surface bicarbonate species. Interestingly, CO_2 is not only interacting with Mg−OH (Ba−OH) groups but also with hydroxyl species characterized by a band at 3773 cm^{-1}.

According to Knözinger and Ratnasamy, OH bands in the high-frequency region of IR spectra of aluminas correspond to OH species exhibiting distinct local environments (determined by the number of Al neighbors in the first coordination sphere of the oxygen atom and the coordination number of the Al atom).[32] The band at 3773 cm^{-1} (type I_a) has been attributed to terminal groups (μ_1) attached to Al_{IV} species.[32,33] In contrast to

(32) Knözinger, H.; Ratnasamy, P. *Catal. Rev.-Sci. Eng.* **1978**, *17*, 31.

(33) Peri, J. B. *J. Phys. Chem.* **1965**, *69*, 211.

this assignment a recent density functional (DFT) study of Digne et al.[34] on hydroxyl groups on γ-alumina surfaces has attributed this band to μ_1-OH groups on Al_{VI} species. The interaction of CO_2 with Mg−OH and Al−OH groups demonstrates that either (i) both species exist close to each other in a distinct chemical environment or (ii) that not only Mg−OH but also μ_1-Al−OH groups possess a basic character. Note that Knözinger and Ratnasamy have already pointed out the basic character of μ_1-Al_{IV}−OH groups responsible for the I_a band at 3773 cm^{-1} in γ-alumina.[32] In agreement with other authors (ref 32 and references therein) they have observed a perturbation of the IR band near 3780 cm^{-1} and the generation of bicarbonate species upon the adsorption of CO_2 on γ-alumina surfaces. Interestingly, for Al_2O_3−MCM-36 no formation of (bi)-carbonates has been observed, indicating that no basic type I_a Al−OH groups are present in this material. The formation of such sites seems to be facilitated by the presence of alkaline earth oxides (MgO, BaO) creating MgO−Al_2O_3 or BaO−Al_2O_3 pillars. As demonstrated by ^{27}Al-MAS NMR measurements, in the MgO and BaO containing defect spinel-type clusters aluminum ions on octahedral *and* tetrahedral interstitial sites are present, whereas for Al_2O_3−MCM-36 mainly octahedrally coordinated aluminum has been determined. The absence of the band assigned to basic type I_a hydroxyl groups on the Al_2O_3−MCM-36 sample strongly supports the assignment of this band to tetrahedrally coordinated Al_{IV}-OH as suggested by Knözinger and Ratnasamy. As a consequence of fundamental interest for catalytic applications our study shows that the intercalation of magnesium (barium) aluminates generates (defect) spinel clusters in the interlayer space with two basic sites: (i) Mg−OH and (ii) μ_1-Al_{IV}−OH groups. It has to be underlined that in contrast to the above-described observations, for the parent (reference) material MCM-22, SiO_2−MCM-36, and Al_2O_3−MCM-36 no formation of carbonate species is detected upon adsorption of CO_2. For Na−MCM-22 only a band at 2356 cm^{-1} can be observed which is characteristic of the stretching vibration of CO_2 linearly adsorbed on Na^+ cations, because the basic character of the reference material is too weak to form carbonates.

Conclusions

Exfoliation of the zeolite layers of the uncalcined precursor of MCM-22 and intercalation of various (aluminum) oxides leads to derivatives of MCM-36 with tunable physicochemical properties. Aluminum ions in the oxide pillars are mainly octahedrally and pentahedrally coordinated. For MgO(BaO)−Al_2O_3−MCM-36 additional aluminum species in a tetrahedral coordination sphere have been determined. These Al ions are probably found on interstitial tetrahedral sites in the (defect) spinel-type oxide clusters between the zeolite layers. The acidic and basic properties of the materials can be modified by the selection of appropriate oxide phases. In addition to Brønsted acid sites in the zeolite sheets, enhanced Lewis acidity is generated by pillaring with (mixed) aluminum oxides. Pyridine adsorption followed by IR spectroscopy and temperature-programmed desorption of ammonia show that, while the concentration of Brønsted acid sites remains constant, the number of Lewis acid sites increases. In comparison to the not-pillared parent material MCM-22, the adsorption of sterically demanding probe molecules such as 2.6-di-tert-butyl-pyridine (2.6-DTBPy) demonstrates for all materials enhanced accessibility of the acid sites on the pore mouth or the outer surface of the zeolite layers. Interestingly, for (MgO/BaO)−Al_2O_3−SiO_2−MCM-36 additional Brønsted acid sites of higher strength are observed. These sites are readily accessible for 2.6-DTBPy and are assigned to the silica−alumina clusters in the interlayer galleries because the synthesis of the materials involves the hydrolysis of tetraethoxysilane (TEOS) with aluminum chloride containing pillaring solutions. Basic properties are introduced by the incorporation of alkaline earth aluminates (MgO/BaO−Al_2O_3) into the interlayer space. Two basic hydroxyl sites have been identified by CO_2 adsorption: (i) Mg(Ba)−OH and (ii) Al_{IV}−OH groups on the spinel-type oxide clusters. The latter basic sites are attributed to hydroxyl groups on aluminum ions in a tetrahedral coordination sphere. As the presence of defect spinel-type oxide clusters seems to be a prerequisite for the formation of these sites, they are only generated if MgO and BaO are used in the synthesis process and have not been detected in Al_2O_3−MCM-36.

Acknowledgment. Financial support of the European Union (Project G1RD-CT99-0065-"DENOXPRO") and the "Dr.-Ing. Leonhard Lorenz Stiftung" is gratefully acknowledged. Special thanks go to Dipl.-Chem. H. Dathe for XRD measurements and Dr. L. Simon for measuring the TEM micrographs. We are thankful to Dipl.-Ing. (FH) F.-X. Hecht and Dipl.-Ing. (FH) M. Neukamm for measuring nitrogen adsorption isotherms and performing AAS elemental analyses.

CM0349607

(34) Digne, M.; Sautet, P.; Raybaud, P.; Euzen, P.; Toulhoat, H. *J. Catal.* **2002**, *211*, 1.